# Experimental report

05/01/2016

**Proposal:** 5-32-808 **Council:** 10/2014

**Title:** Characterisation of partial magnetic order in Gd2Sn2O7

**Research area:** Physics

**This proposal is a new proposal**


**Main proposer:** John Ross STEWART

**Experimental team:** Jason S. GARDNER
John Ross STEWART

**Local contacts:** Andrew WILDES


**Samples:** Gd2Sn2O7

| Instrument | Requested days | Allocated days | From | To |
|---|---|---|---|---|
| D7 | 5 | 5 | 29/07/2015 | 03/08/2015 |


## Abstract:

We have recently performed a WISH experiment on polycrystalline Gd2Sn2O7 as a function of field. The zero field low-temperature magnetic structure was thought to correspond to that predicted by Palmer and Chalker, being a 4-sublattice k=0 antiferromagnet. However our WISH data do not agree with this model, and furthermore it appears as if half the full Gd moment is disordered, as evidenced by weaker-than-expected Bragg intensities, and considerable diffuse scattering. We now propose to study the disordered magnetic structure using polarization analysis on D7. We will need 5 days for this measurement.

# Analysis of Paramagnetic Diffuse Scattering in $Gd_2Sn_2O_7$

I analysed the magnetic diffuse-scattering data for $Gd_2Sn_2O_7$ using two approaches. First, I used reverse Monte Carlo (RMC) refinement [1, 2], which uses the Metropolis algorithm to fit spin configurations directly to the experimental diffuse-scattering data. The "cost function" minimised during the refinement is given by

$$\chi^2 = W \sum_Q \left[ \frac{I_{\mathrm{calc}}(Q) - I_{\mathrm{expt}}(Q)}{\sigma(Q)} \right]^2, \tag{1}$$

where $I(Q)$ is the magnetic diffuse neutron-scattering intensity at reciprocal-space position $Q$, subscript "calc" and "expt" denote calculated and experimental intensities respectively, $\sigma(Q)$ is the experimental uncertainty, and $W$ is an empirical weighting factor which determines how closely the algorithm will attempt to fit the data. The powder-averaged magnetic diffuse-scattering intensity is calculated from the equation [3]

$$I(Q) = C\,[g f(Q)]^2 \left\{ \frac{2}{3} + \frac{1}{N} \sum_{j \neq i} \left[ A_{ij} \frac{\sin Q r_{ij}}{Q r_{ij}} + B_{ij} \left( \frac{\sin Q r_{ij}}{(Q r_{ij})^3} - \frac{\cos Q r_{ij}}{(Q r_{ij})^2} \right) \right] \right\}, \tag{2}$$

where $f(Q)$ is the $Gd^{3+}$ magnetic form factor and $C = (\gamma_n r_e/2)^2 = 0.07265$ barn is a constant. The spin correlation coefficients $A_{ij}$ and $B_{ij}$ are given by

$$\begin{aligned} A_{ij} &= \mathbf{S}_i \cdot \mathbf{S}_j - (\mathbf{S}_i \cdot \hat{\mathbf{r}}_{ij})(\mathbf{S}_j \cdot \hat{\mathbf{r}}_{ij}) \\ B_{ij} &= 3(\mathbf{S}_i \cdot \hat{\mathbf{r}}_{ij})(\mathbf{S}_j \cdot \hat{\mathbf{r}}_{ij}) - \mathbf{S}_i \cdot \mathbf{S}_j, \end{aligned} \tag{3}$$

where $\mathbf{r}_{ij} = \mathbf{r}_j - \mathbf{r}_i$ is the vector connecting $Gd^{3+}$ spins $\mathbf{S}_i$ and $\mathbf{S}_j$ with magnitude $r_{ij} = |\mathbf{r}_j - \mathbf{r}_i|$, and the unit vector $\hat{\mathbf{r}}_{ij} = \mathbf{r}_{ij}/r_{ij}$. The RMC approach does not give any direct information about the spin Hamiltonian, but instead yields the most disordered spin configurations compatible with the following three constraints: the experimental diffuse-scattering data, the pyrochlore lattice occupied by the $Gd^{3+}$ ions, and the fixed length of the $Gd^{3+}$ spins.

Second, I compare the RMC results with the predictions of the minimal interaction model for $Gd_2Sn_2O_7$[4], given by the spin Hamiltonian

$$H = -\frac{J_1}{2} \sum_{\langle i,j \rangle} \mathbf{S}_i \cdot \mathbf{S}_j + \frac{D}{2} \sum_{i,j} \frac{\mathbf{S}_i \cdot \mathbf{S}_j - 3(\mathbf{S}_i \cdot \hat{\mathbf{r}}_{ij})(\mathbf{S}_j \cdot \hat{\mathbf{r}}_{ij})}{(r_{ij}/r_1)^3} \tag{4}$$

$$= H_{\mathrm{exchange}} + H_{\mathrm{dipolar}}. \tag{5}$$

Here, $\mathbf{S}_i$ are classical $Gd^{3+}$ spins of magnitude $\sqrt{S(S+1)}$ with $S = 7/2$. The antiferromagnetic nearest-neighbour exchange interaction is denoted $J_1$; literature values are $J_1 = -0.25$ K [5] and $J_1 = -0.216$ K [6]. The magnitude of the magnetic dipolar interaction at the nearest-neighbour distance $r_1$ is given by

$$\begin{aligned} D &= \frac{\mu_0 (g\mu_B)^2}{4\pi r_1^3 k_B} \\ &= 0.049\,\mathrm{K}. \end{aligned}$$

I used a Metropolis Monte Carlo algorithm to simulate Eq. (4). The long-range nature of the dipolar interaction was handled using Ewald summation [7] and the time needed to equilibrate the simulations was estimated using the spin autocorrelation function. All simulations were performed using spin configurations of size $6 \times 6 \times 6$ conventional unit cells (3456 spins), and 20 separate simulations were averaged to generate the results shown below.

## 2 $Gd_2Sn_2O_7$: results

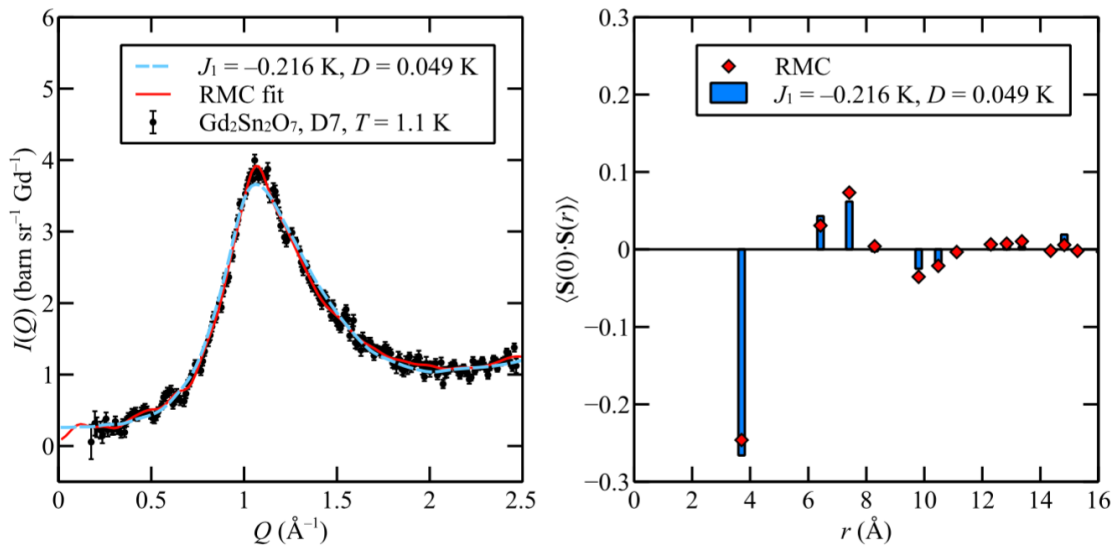


(a) (b)

Figure 1: (a) Experimental diffuse-scattering data for $Gd_2Sn_2O_7$ ,collected using the D7 diffractometer at $T = 1.1\,\mathrm{K}$ (black circles), reverse Monte Carlo fit (solid red line), and calculation for the $J_1 + D$ Hamiltonian [Eq. (4)] at $T = 1.1\,\mathrm{K}$ (blue dashed line). (b) Radial spin correlation function $\langle \mathbf{S}(0) \cdot \mathbf{S}(r) \rangle$ calculated from RMC refinement (red diamonds) and from the $J_1 + D$ Hamiltonian (blue bars).

Fig. 1(a) shows the experimental diffuse-scattering data for $Gd_2Sn_2O_7$ ,collected using the D7 diffractometer at $T = 1.1\,\mathrm{K}$, the RMC fit to data, and the calculation for the $J_1 + D$ Hamiltonian [Eq. (4)] at $T = 1.1\,\mathrm{K}$ with $J_1 = -0.216\,\mathrm{K}$ and $D = 0.049\,\mathrm{K}$ (similar results were obtained for $J_1 = -0.25\,\mathrm{K}$ and $D = 0.049\,\mathrm{K}$ [5]). The $J_1 + D$ calculation is scaled vertically to match the experimental data. The good agreement between the experimental data and the $J_1 + D$ model suggests that further-neighbour exchange interactions are very small in $Gd_2Sn_2O_7$ . Fig. 5(b) shows the radial spin-correlation function determined from RMC refinement and the $J_1 + D$ model.

Fig. 2 shows stereographic projections of the probability distribution of spin orientations. These stereographic projection are expressed in terms of the number of spins $n(\theta, \phi)$ which lie within the angular range $\mathrm{d}\theta, \mathrm{d}(\cos\phi)$,

$$\ln(p) = \ln\left[\frac{n(\theta,\phi)}{NZ\mathrm{d}\theta\,\mathrm{d}(\cos\phi)}\right], \tag{6}$$

where $Z$ is the number of spin configurations and $N$ the number of spins per configuration. The $\mathbf{z}$ axis in Fig. 2 is the local $\langle 111 \rangle$ axis for a given $Gd^{3+}$ ion, and $\mathbf{x} \in \langle 112 \rangle$ and $\mathbf{y} \in \langle 110 \rangle$ axes are chosen to be orthogonal to $\mathbf{z}$. Both the RMC refinements and the simulations of the $J_1 + D$ model show a preference for spins to lie within the plane perpendicular to the local $\langle 111 \rangle$ axis at $T = 1.1\,\mathrm{K}$, which was previously suggested by ESR measurements [8]. The

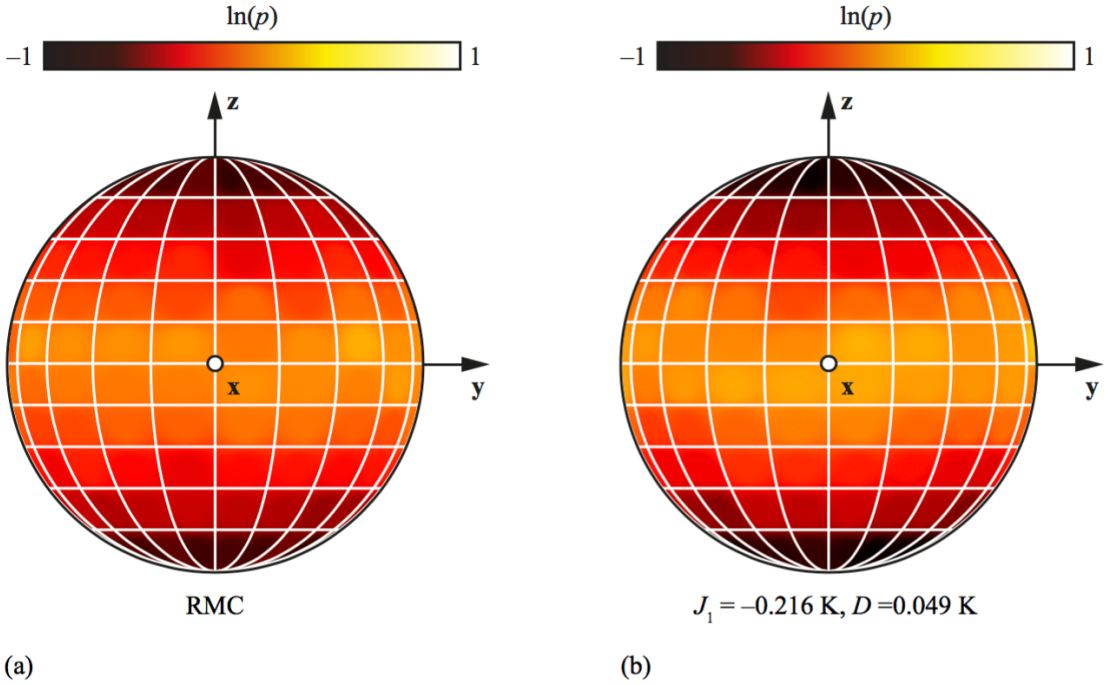


Figure 2: Stereographic projections of the logarithmic probability distribution function $\ln(p)$ of spin orientations obtained from (a) RMC refinement to neutron-scattering data for $Gd_2Sn_2O_7$, and (b) $J_1 + D$ model [Eq. (4)].

similarity between the RMC results and the $J_1 + D$ model suggests that the magnetic anisotropy is due mostly to the long-ranged dipolar interaction, rather than to crystal-field effects.

Fig. 3 shows the three-dimensional spin correlation function $\langle \mathbf{S}(\mathbf{0}) \cdot \mathbf{S}(\mathbf{r}) \rangle$. Compared to Fig. 1(b), this shows that spin correlations are of much greater magnitude for the third neighbours labelled $\mathbf{r}_{3a}$ than the third neighbours labelled $\mathbf{r}_{3b}$.

Fig. 4 shows the single-crystal magnetic diffuse-scattering intensity,

$$I(\mathbf{Q}) \propto [f(Q)]^2 \sum_{i,j} \mathbf{S}_i^{\perp} \cdot \mathbf{S}_j^{\perp} \exp\left[\mathrm{i}\mathbf{Q} \cdot (\mathbf{r}_j - \mathbf{r}_i)\right],$$

where $\mathbf{S}^{\perp} = \mathbf{S} - \mathbf{Q}\,(\mathbf{S} \cdot \mathbf{Q})\,/Q^2$ is the component of spin perpendicular to $\mathbf{Q}$. The calculated $I(\mathbf{Q})$ from RMC refinement to the powder data closely resembles the $J_1 + D$ model calculation. Both calculations indicate a build-up of scattering intensity near to integer-$hkl$ positions, consistent with the incipient $\mathbf{k} = 0$ magnetic propagation vector.

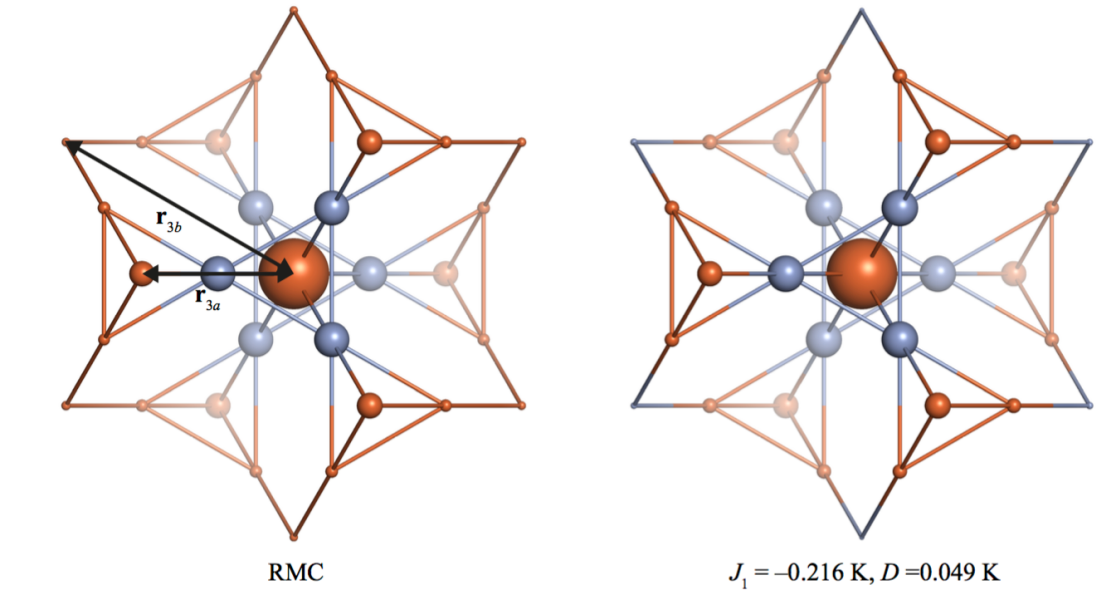


Figure 3: Three-dimensional spin correlation function $\langle \mathbf{S}(\mathbf{0}) \cdot \mathbf{S}(\mathbf{r}) \rangle$ for (a) RMC refinement to neutron-scattering data for $Gd_2Sn_2O_7$, and (b) $J_1 + D$ model [Eq. (4)]. Both images are viewed down the local $\langle 111 \rangle$ axis and show the coordination environment of each $Gd^{3+}$ion. Ferromagnetic correlations ($\langle \mathbf{S}(\mathbf{0}) \cdot \mathbf{S}(\mathbf{r}) \rangle > 0$) are shown as brown spheres, and antiferromagnetic correlations ($\langle \mathbf{S}(\mathbf{0}) \cdot \mathbf{S}(\mathbf{r}) \rangle < 0$) are shown as blue spheres. The radius of each sphere is proportional to $\sqrt{|\langle \mathbf{S}(\mathbf{0}) \cdot \mathbf{S}(\mathbf{r}) \rangle|}$.

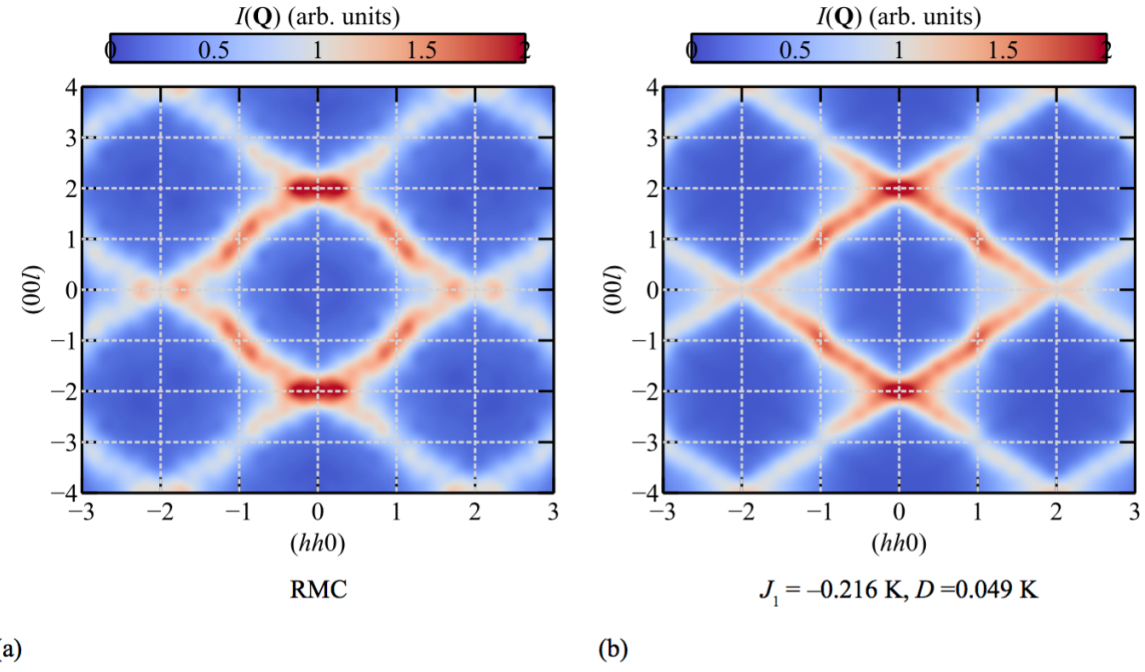


Figure 4: Single-crystal magnetic diffuse scattering patterns $I(\mathbf{Q})$ calculated from (a) RMC refinement to neutron-scattering data for $Gd_2Sn_2O_7$, and (b) $J_1 + D$ model [Eq. (4)]. Both images show the $(hhl)$ reciprocal-space plane.